

A comparative study of the electrochemical and proton-reduction behaviour of diphosphine-dithiolate complexes $[M_2(CO)_4(\mu\text{-dppm})\{\mu\text{-S}(\text{CH}_2)_n\text{S}\}]$ ($M = \text{Fe, Ru}; n = 2, 3$)

Shishir Ghosh^{1,2} · Shariff E. Kabir¹ · Graeme Hogarth² 

Received: 19 June 2017 / Accepted: 6 July 2017 / Published online: 24 July 2017
© The Author(s) 2017. This article is an open access publication

Abstract The electrochemistry of dppm-bridged dithiolate complexes $[M_2(CO)_4(\mu\text{-dppm})\{\mu\text{-S}(\text{CH}_2)_n\text{S}\}]$ ($M = \text{Fe, Ru}; n = 2, 3$) has been studied by cyclic voltammetry. The diiron complexes show similar electrochemical responses in CH_2Cl_2 but differ significantly in MeCN, while the diruthenium complexes change only slightly with changes in the dithiolate backbone and solvent. Proton-reduction studies in MeCN with $\text{HBF}_4 \cdot \text{Et}_2\text{O}$ as the proton source show that all are active catalysts for proton reduction in their singly reduced state. An additional catalytic event is observed for all, resulting from their partial protonation giving $[M_2(CO)_4(\mu\text{-dppm})\{\mu\text{-S}(\text{CH}_2)_n\text{S}\}(\mu\text{-H})][\text{BF}_4]$. The diiron complexes show better long-term stability to acids, the diruthenium complexes degrading at high acid concentrations.

Introduction

Dithiolate-bridged diiron complexes of the type $[\text{Fe}_2(\text{CO})_6(\mu\text{-dithiolate})]$ have been intensely studied [1–19] due to their structural resemblance with the two-iron unit of the

H-cluster active site of $[\text{FeFe}]$ -hydrogenases, enzymes that catalyse the reversible interconversion of protons–electrons and hydrogen. A key step in electrocatalytic proton reduction is protonation of the diiron centre, but $[\text{Fe}_2(\text{CO})_6(\mu\text{-dithiolate})]$ complexes are not basic enough to undergo protonation except by extremely strong acids [20–22]. To increase the basicity of the diiron centre, one or more carbonyls can be substituted by more electron-donating ligands such as phosphines or cyanide [23–52]. Diphosphines have been widely used in this context and can either bridge the diiron centre or chelate to one end, bridging complexes, $[\text{Fe}_2(\text{CO})_4(\mu\text{-diphosphine})(\mu\text{-dithiolate})]$ being thermodynamically stable with respect to isomeric chelate complexes $[\text{Fe}_2(\text{CO})_4(\kappa^2\text{-diphosphine})(\mu\text{-dithiolate})]$. Consequently a large number of diphosphine-bridged diiron-dithiolate complexes have been reported [23–32] but surprisingly little attention has been paid to their proton-reduction chemistry [27–32] even though some, for example $[\text{Fe}_2(\text{CO})_4(\mu\text{-dppf})(\mu\text{-pdt})]$ (dppf = 1,1'-bis(diphenylphosphino)ferrocene), have been shown to be efficient proton-reduction catalysts [29]. Similarly, given the large number of diiron complexes tested as proton-reduction catalysts, related diruthenium complexes have not been widely studied [53–56]. Herein we detail a comparative investigation of the electrochemistry and proton-reduction behaviour of diiron and diruthenium complexes $[\text{M}_2(\text{CO})_4(\mu\text{-dppm})(\mu\text{-pdt})]$ [24, 27, 57] and $[\text{M}_2(\text{CO})_4(\mu\text{-dppm})(\mu\text{-edt})]$ [26, 27, 57] (Fig. 1).

Electronic supplementary material The online version of this article (doi:10.1007/s11243-017-0164-6) contains supplementary material, which is available to authorized users.

✉ Shishir Ghosh
sghosh_006@yahoo.com

✉ Graeme Hogarth
graeme.hogarth@kcl.ac.uk

¹ Department of Chemistry, Jahangirnagar University, Savar, Dhaka 1342, Bangladesh

² Department of Chemistry, King's College London, Britannia House, 7 Trinity Street, London SE1 1DB, UK

Experimental

Complexes 1–4 were prepared according to published methods [24, 26, 27, 57] (see ESI for details). IR spectra were recorded on a Nicolet 6700 FT-IR spectrometer in a solution cell fitted with calcium fluoride plates, subtraction

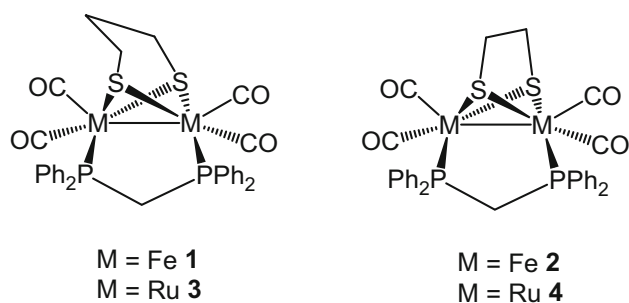


Fig. 1 Diiron and diruthenium complexes $[\text{M}_2(\text{CO})_4(\mu\text{-pdt})]$ and $[\text{M}_2(\text{CO})_4(\mu\text{-edt})]$

of the solvent absorptions being achieved by computation. Electrochemistry was carried out in either deoxygenated dichloromethane or in deoxygenated MeCN with 0.1 M TBAPF₆ as supporting electrolyte. The working electrode was a 3-mm-diameter glassy carbon electrode which was polished with 0.3 μm alumina slurry prior to each scan. The counter electrode was a Pt wire, and the quasi-reference electrode was a silver wire. All CVs were referenced to the Fc/Fc⁺ redox couple. An Autolab potentiostat (EcoChemie, Netherlands) was used for all electrochemical measurements. Catalysis studies were carried out by adding equivalents of HBF₄·Et₂O (Sigma-Aldrich).

Results and discussion

Electrochemical studies

The electrochemical response of **1–4** has been studied by cyclic voltammetry (CV) both in CH₂Cl₂ and in MeCN. CVs of $[\text{Fe}_2(\text{CO})_4(\mu\text{-dppm})(\mu\text{-pdt})]$ (**1**) and $[\text{Fe}_2(\text{CO})_4(\mu\text{-dppm})(\mu\text{-edt})]$ (**2**) in CH₂Cl₂ (scan rate 0.1 V/s) are shown in Fig. 2. Complex **1** shows a quasi-reversible oxidation at $E_{1/2} = 0.18$ V ($\Delta E = 0.10$ V) followed by two irreversible oxidations at $E_p = 0.49$ V and $E_p = 0.71$ V. The first oxidation shows good chemical reversibility ($i_p^{\text{red}}/i_p^{\text{ox}} = \sim 1$) when the potential is cycled below 0.4 V and remains reversible at all scan rates (0.025–1 V/s) (Fig. S1a). A plot of the oxidative peak current against square root of the scan rate gives a straight line, indicating that this originates from a diffusion-controlled solution process (Fig. 1Sb). It also displays an irreversible reduction near the negative limit of the potential window at $E_p = -2.57$ V (Table 1). CVs of **2** show similar features (Fig. 2); a quasi-reversible oxidation at $E_{1/2} = 0.39$ V ($\Delta E = 0.11$ V), the reversibility of which is maintained at all scan rates (0.025–1 V/s) and shows good chemical reversibility when the potential is cycled below 0.55 V (Fig. S2), followed by a broad irreversible oxidative wave at $E_p = 0.59$ V and an irreversible reduction at $E_p = -2.52$ V. CVs of both show additional oxidative and

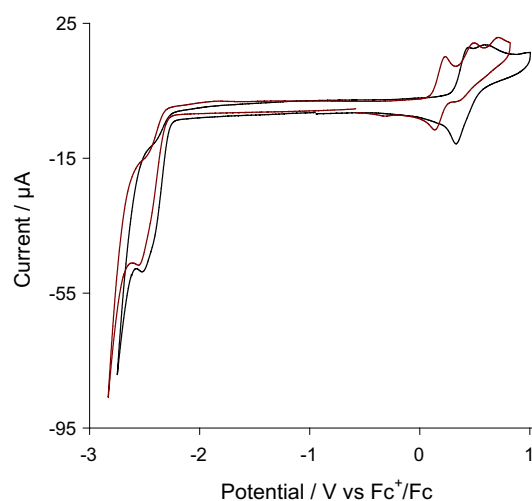


Fig. 2 CVs of $[\text{Fe}_2(\text{CO})_4(\mu\text{-dppm})(\mu\text{-pdt})]$ (**1**) (brown) and $[\text{Fe}_2(\text{CO})_4(\mu\text{-dppm})(\mu\text{-edt})]$ (**2**) (black) in CH₂Cl₂ (1 mM solution, supporting electrolyte $[\text{NBu}_4][\text{PF}_6]$, scan rate 0.1 V/s, glassy carbon electrode, potential versus Fc⁺/Fc). (Color figure online)

Table 1 First oxidation and reduction potentials of **1–4** in CH₂Cl₂ and MeCN

Compounds	In CH ₂ Cl ₂		In MeCN	
	$E_p^{\text{red1}}/\text{V}$	$E_p^{\text{ox1}}/\text{V}$	$E_p^{\text{red1}}/\text{V}$	$E_p^{\text{ox1}}/\text{V}$
$[\text{Fe}_2(\text{CO})_4(\mu\text{-dppm})(\mu\text{-pdt})]$ (1)	-2.57	0.18*	-2.20	0.24
$[\text{Fe}_2(\text{CO})_4(\mu\text{-dppm})(\mu\text{-edt})]$ (2)	-2.52	0.39*	-2.18*	0.30
$[\text{Ru}_2(\text{CO})_4(\mu\text{-dppm})(\mu\text{-pdt})]$ (3)	–	0.23	-2.45	0.21
$[\text{Ru}_2(\text{CO})_4(\mu\text{-dppm})(\mu\text{-edt})]$ (4)	–	0.35	-2.43	0.27

* $E_{1/2}$ value

reductive features at higher scan rates (≥ 0.25 V/s) attributed to products generated from the irreversible reductive and oxidative processes (Figs. S3, S4).

In contrast to their iron analogues, CVs of ruthenium complexes $[\text{Ru}_2(\text{CO})_4(\mu\text{-dppm})(\mu\text{-pdt})]$ (**3**) and $[\text{Ru}_2(\text{CO})_4(\mu\text{-dppm})(\mu\text{-edt})]$ (**4**) in CH₂Cl₂ show only a sharp irreversible oxidation peak followed by a small quasi-reversible oxidation (Fig. 3). No reduction peak was observed for either within the potential window of CH₂Cl₂. The irreversible oxidation peak of **3** appears at $E_p = 0.23$ V, followed by a small quasi-reversible oxidation at $E_{1/2} = 0.68$ V ($\Delta E = 0.11$ V), while for **4** oxidative peaks appear at $E_p = 0.35$ V and $E_{1/2} = 0.78$ V ($\Delta E = 0.13$ V), respectively. The first oxidation peak of both does not show any reversibility at all scan rates even when cycled below 0.60 V for **3** and 0.65 V for **4** (Figs. S5, S6). The CVs also display two small reductive features on the return scan ($E_p = -0.59$ V and $E_p = -0.42$ V for **3**; $E_p = -0.46$ V and $E_p = -0.22$ V for **4**) associated with the product(s) of the first oxidation.

The electrochemistry of **1** has been studied previously in MeCN (in 50 mM $[\text{NBu}_4][\text{PF}_6]$) using Ag/Ag⁺ as the

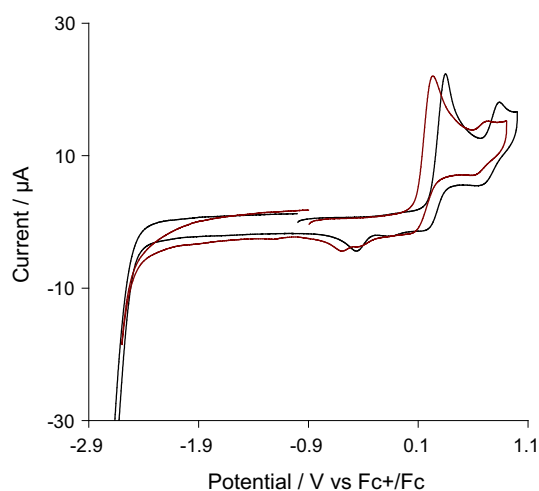


Fig. 3 CVs of $[\text{Ru}_2(\text{CO})_4(\mu\text{-dppm})(\mu\text{-pdt})]$ (**3**) (brown) and $[\text{Ru}_2(\text{CO})_4(\mu\text{-dppm})(\mu\text{-edt})]$ (**4**) (black) in CH_2Cl_2 (1 mM solution, supporting electrolyte $[\text{NBu}_4][\text{PF}_6]$, scan rate 0.1 V/s, glassy carbon electrode, potential versus Fc^+/Fc). (Color figure online)

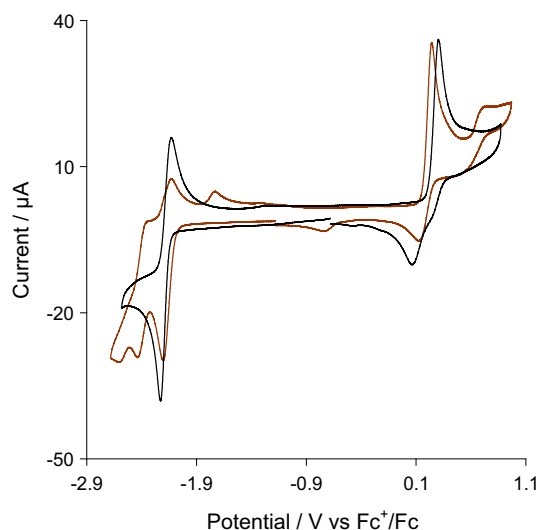


Fig. 4 CVs of $[\text{Fe}_2(\text{CO})_4(\mu\text{-dppm})(\mu\text{-pdt})]$ (**1**) (brown) and $[\text{Fe}_2(\text{CO})_4(\mu\text{-dppm})(\mu\text{-edt})]$ (**2**) (black) in MeCN (1 mM solution, supporting electrolyte $[\text{NBu}_4][\text{PF}_6]$, scan rate 0.1 V/s, glassy carbon electrode, potential versus Fc^+/Fc). (Color figure online)

reference electrode [27]. For accurate comparison, we also carried out its electrochemistry in 100 mM $n\text{-Bu}_4\text{NPF}_6$ in MeCN using Fc/Fc^+ couple as the reference and found that the results are very similar to those reported previously [27]. Electrochemical behaviour of **1** and **2** in MeCN is not only very different than that observed in CH_2Cl_2 , but CVs show that **1** and **2** vary significantly in this solvent (Fig. 4). Thus **1** shows a large oxidation peak at $E_p = 0.24$ V, followed by a smaller oxidation peak at $E_p = 0.70$ V, while **2** shows only one oxidative response at $E_p = 0.30$ V. Both oxidative processes of **1** exhibit some reversibility when

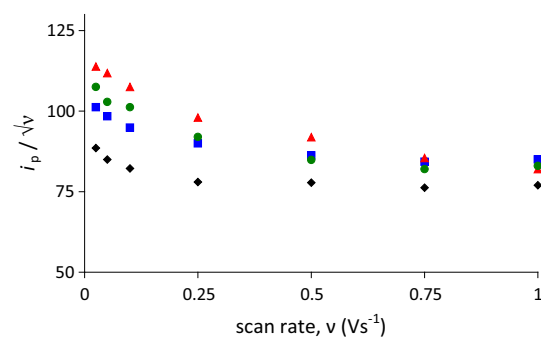


Fig. 5 Scan rate (v) dependence of the current function (i_p/\sqrt{v}) for the reduction of **1** (black diamonds), **2** (blue squares), **3** (red triangles) and **4** (green spheres) (1 mM solution in MeCN, supporting electrolyte $[\text{NBu}_4][\text{PF}_6]$, glassy carbon electrode). (Color figure online)

the scan rate is varied (0.025–1 V/s), whereas that of **2** remains irreversible, displaying a reductive response at $E_p = 0.07$ V on the return scan attributed to the reduction of a product formed after irreversible oxidation (Figs. S7, S8). Complex **1** shows three reduction peaks at $E_p = -2.20$, -2.44 , -2.61 V, respectively, in contrast **2** displays only a quasi-reversible reduction within the potential limit at $E_{1/2} = -2.18$ V ($\Delta E = 0.10$ V), the peak current ratio ($i_p^{\text{red}}/i_p^{\text{ox}}$) of ca. 0.8 indicating good chemical reversibility. The first reduction peak on the CV of **1** has some reversibility at scan rates of 0.1 V/s and this increases if the potential is cycled below -2.3 V (Fig. S9). However, scan rate variation shows that the reversibility of this and the second reductive process also increases at higher scan rates (Figs. S7, S10). The small oxidative feature at $E_p = -1.73$ V on the return scan, which is not observed when the potential is cycled below -2.3 V, can be attributed to oxidation of the product generated by second and third reductive processes (Fig. S9). The reduction peak at $E_p = -0.74$ V and the oxidative response at $E_p = -1.26$ V, which becomes prominent at higher scan rates, are associated with the first oxidative and reductive processes of **1**, respectively. In contrast CVs of **2** do not show any additional feature as the scan rate is varied (Fig. S8). Reduction of **2** and the first reduction process of **1** are diffusion-controlled solution processes as confirmed by plotting the reductive peak currents against square root of the scan rates which give straight lines passing through the origin (Fig. S10, S11). The current function (i_p/\sqrt{v}) associated with these processes show a slight deviation from linearity at slow scan rates (Fig. 5), which indicates that more than one electron may be involved in the electro process on longer time scales.

Earlier CVs of **1** in MeCN showed only one reduction wave as experiments were carried out with a comparatively smaller potential window than used in this study [27]. In our experiment, we saw three consecutive reduction waves for **1** with small gaps between the peaks (~ 0.2 V)

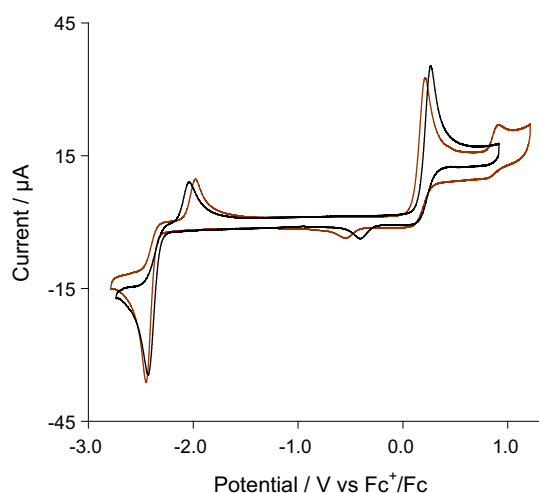


Fig. 6 CVs of $[\text{Ru}_2(\text{CO})_4(\mu\text{-dppm})(\mu\text{-pdt})]$ (**3**) (brown) and $[\text{Ru}_2(\text{CO})_4(\mu\text{-dppm})(\mu\text{-edt})]$ (**4**) (black) in MeCN (1 mM solution, supporting electrolyte $[\text{NBu}_4][\text{PF}_6]$, scan rate 0.1 V/s, glassy carbon electrode, potential versus Fc^+/Fc). (Color figure online)

suggesting that the second reduction does not correspond to an $\text{Fe(I)Fe(0)} \rightarrow \text{Fe(0)Fe(0)}$ process, for which a large potential gap between the first and second reduction peaks should be observed. We speculate that the second reduction is occurring from a solvent stabilized species, possibly $[\text{Fe}_2(\text{CO})_3(\text{NCMe})(\mu\text{-dppm})(\mu\text{-pdt})]$ generated from the radical chain reaction propagated by loss of a CO from the reduced species $\mathbf{1}^-$ with subsequent uptake of a MeCN molecule followed by electron transfer to another molecule of **1**. This process is well established for mononuclear 18-electron carbonyl complexes and has also been observed for the parent hexacarbonyl $[\text{Fe}_2(\text{CO})_6(\mu\text{-pdt})]$ [11]. We are uncertain of the origin of the third reduction wave of **1**. It may result from reduction of $\mathbf{1}^-$ to $\mathbf{1}^{2-}$ or a second electron input to the solvent stabilized species. Unlike **1**, the single reversible reductive response displayed by **2** is indicative of its resistance to CO loss in its singly reduced state, i.e. $\mathbf{2}^-$ is significantly more stable to CO loss than $\mathbf{1}^-$ in MeCN.

In contrast, diruthenium complexes **3** and **4** show very similar electrochemical responses in MeCN (Fig. 6); CVs display an oxidation ($E_p = 0.21$ V for **3** and $E_p = 0.27$ V for **4**) and a reduction ($E_p = -2.45$ V for **3** and $E_p = -2.43$ V for **4**) which are irreversible at all scan rates (Figs. S12, S13). They also show additional reductive ($E_p = -0.54$ V for **3** and $E_p = -0.40$ V for **4**) and oxidative ($E_p = -1.98$ V for **3** and $E_p = -2.04$ V for **4**) features on return scans due to the reduction and oxidation of products generated during the forward scan (Fig. 6). Complex **3** also shows a small second oxidative response at $E_p = 0.91$ V on the forward scan which is only observed on the CV of **4** (at $E_p = 0.75$ V) at scan rate ≤ 0.025 V/s. Plots of current function (i_p/\sqrt{v}) associated with the

reduction of **3** and **4** against scan rates show a slight deviation from linearity only at slow scan rates (Fig. 5) indicating that more than one electron may be involved in the electrode process on longer time scales; otherwise, the reductions of **3** and **4** are one electron processes.

From the above results, it is clear that solvent has a significant influence on the electrochemical response of the diiron complexes **1–2**. The pattern of their CVs is very similar in CH_2Cl_2 , but quite different in MeCN indicating that a change in the dithiolate backbone has a pronounced effect on their electrochemical stabilities. In contrast, if we overlook the absence of a reduction wave in the CVs in CH_2Cl_2 , the gross features of the CVs of **3–4** are similar in both solvents. The reason for the absence of a reduction wave in CH_2Cl_2 can be explained by the following factors; (i) the cathodic window of CH_2Cl_2 is smaller as compared to MeCN and (ii) ionic species formed upon redox reactions are better stabilized in MeCN rather than in CH_2Cl_2 . The experimental data are also in accord with this as both **3** and **4** undergo oxidation at less positive potential in MeCN compared to that observed in CH_2Cl_2 (Table 1).

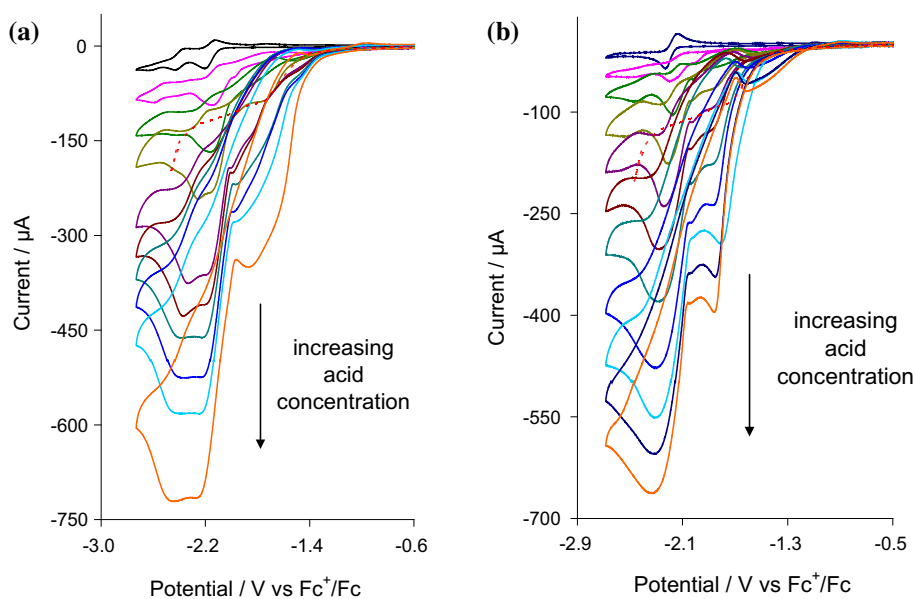
Electrocatalytic studies

The electrocatalytic proton-reduction ability of **1–4** has been studied in MeCN using $\text{HBF}_4 \cdot \text{Et}_2\text{O}$ as the proton source. In the presence of acid, the first reductions of **1–4** are electrocatalytic with respect to proton reduction as evident from the voltammetry (Figs. 7, 8, S14–S17).

The current of the first reduction wave of **1** increases on sequential addition of molar equivalents of acid and separates into two distinct catalytic waves (ca. -2.2 and -2.4 V) at higher acid concentrations (Fig. 7a). This phenomenon has been observed by Pickett and co-workers for the parent hexacarbonyl $[\text{Fe}_2(\text{CO})_6(\mu\text{-pdt})]$ who attributed it to two ECEC processes [11]. We assume that a similar ECEC mechanism is involved in the catalytic cycle of **1** at its first reduction potential (Scheme 1). Thus, reduction of **1** is followed by protonation to generate $\mathbf{1H}$, which undergoes further reduction at the same potential to yield $\mathbf{1H}^-$; protonation of this intermediate then liberates hydrogen via $\mathbf{1H}_2$ and leads to the recovery of **1** accounting for the first catalytic wave (**process I**). However, $\mathbf{1H}_2$ can also be reduced at ca. -2.4 V thus affording $\mathbf{1H}_2^-$, which liberates H_2 to regenerate $\mathbf{1}^-$ and this process accounts for the second catalytic wave (**process II**). Complex **1** has previously been shown to catalyse proton reduction in the presence of $\text{CF}_3\text{SO}_3\text{H}$ at its first reduction potential (ca. -2.1 V versus Ag/AgNO_3) by Sun and co-workers [27] and our observations are in full accord with their results.

Complex **2** shows a single catalytic wave at the potential of its first reduction, consistent with an electrochemically

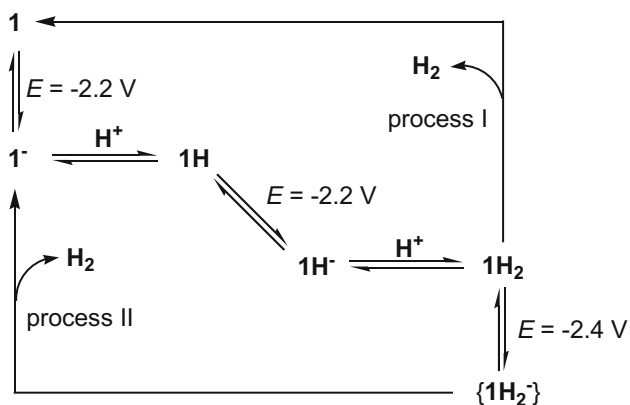
Fig. 7 CVs of **a** $[\text{Fe}_2(\text{CO})_4(\mu\text{-dppm})(\mu\text{-pdt})]$ (**1**) and **b[\text{Fe}_2(\text{CO})_4(\mu\text{-dppm})(\mu\text{-edt})] (**2**) in the absence of acid and in the presence of 1–10 molar equivalents of $\text{HBF}_4\cdot\text{Et}_2\text{O}$ (1 mM solution in acetonitrile, supporting electrolyte $[\text{NBu}_4][\text{PF}_6]$, scan rate 0.1 V/s, glassy carbon electrode, potential versus Fc^+/Fc). Response of 10 equivalents $\text{HBF}_4\cdot\text{Et}_2\text{O}$ alone is shown with the red dotted line. (Color figure online)**



initiated catalytic process (Fig. 7b). It may follow either an ECEC mechanism (**process I**) or a slightly different ECCE mechanism as suggested for related complexes [30, 31, 41, 42]. In the latter, the protonated species (**2H**), formed after initial reduction and subsequent protonation, undergoes a second protonation to yield 2H_2^+ which then takes up a second electron and liberates H_2 . We cannot unambiguously specify a single mechanism for **2** at this juncture which may follow either of these two or both pathways for hydrogen generation. An additional catalytic wave developed for both **1** and **2** at a ca. 0.4 V more positive potential than that of the first reduction wave. Build-up of small amounts of catalytic current at more positive potentials than that of the first reduction wave was also observed by Sun and co-workers while using

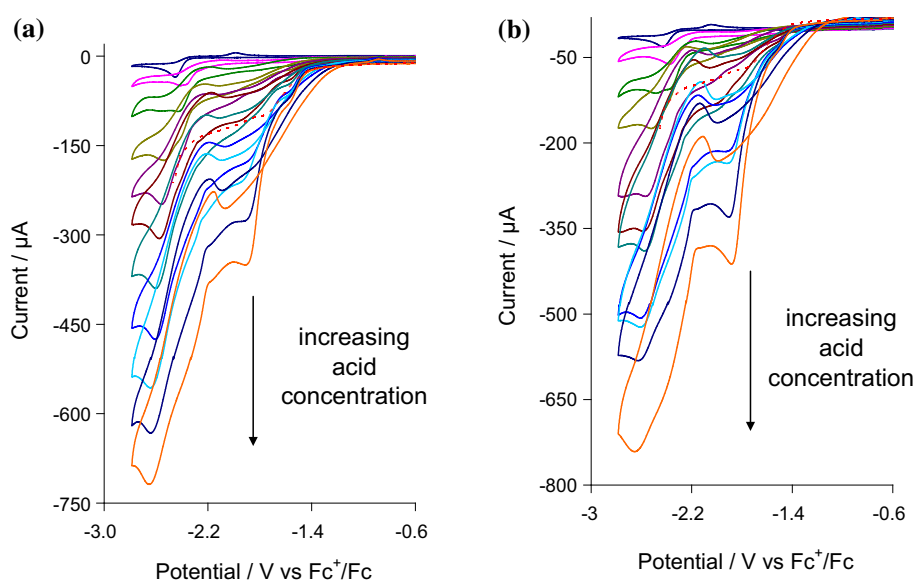
$\text{CF}_3\text{SO}_3\text{H}$ as the proton source [27]. This catalytic wave is well defined for **2** and can be attributed to protonated species 1H^+ and 2H^+ . The oxidation potential(s) of both remain unchanged during catalysis (inset of Figs. S14, S15) which rules out the presence of significant amounts of 1H^+ and 2H^+ in solution, but we suggest that there might be an equilibrium between the neutral and protonated complexes which lies almost entirely to the neutral species at low acid concentrations and shifts slightly as the concentration of acid is increased. To validate this supposition, we monitored changes in their IR spectra with respect to acid concentration. Thus, upon addition of one molar equivalent of acid in CH_2Cl_2 solutions of **1** and **2**, a new set of very weak absorption bands appear at higher wavenumbers in their IR spectra, becoming more intense as the concentration of acid is gradually increased at the expense of the intensity of the bands observed for neutral complexes (Figs. S18, S19). This observation proves that the protonated **1** and **2** are indeed responsible for the catalytic waves seen at more positive potential than their first reduction wave. We speculate a CECE mechanism which is involved for this catalytic event as observed for related complexes [13–15]. However, an attempt to monitor this slow protonation process via NMR spectroscopy was unsuccessful.

Diruthenium complexes **3** and **4** also show similar catalytic waves (Figs. 8, S16, S17) at their first reduction potential. Processes involved in their electrocatalytic proton reduction are difficult to predict due to their less-resolved reduction currents, but we assume one of the two mechanisms described for their iron analogues. Additional catalytic waves at a potential ca. 0.5 V more positive than their first reduction are also noted for **3–4** presumably due



Scheme 1 Proposed mechanism for the electrocatalytic reduction of protons to H_2 by **1**

Fig. 8 CVs of **a** $[\text{Ru}_2(\text{CO})_4(\mu\text{-dppm})(\mu\text{-pdt})]$ (**3**) and **b** $[\text{Ru}_2(\text{CO})_4(\mu\text{-dppm})(\mu\text{-edt})]$ (**4**) in the absence of acid and in the presence of 1–10 molar equivalents of $\text{HBF}_4\cdot\text{Et}_2\text{O}$ (1 mM solution in acetonitrile, supporting electrolyte $[\text{NBu}_4][\text{PF}_6]$, scan rate 0.1 V/s, glassy carbon electrode, potential versus Fc^+/Fc). Response of 10 equivalents $\text{HBF}_4\cdot\text{Et}_2\text{O}$ alone is shown with the red dotted line. (Color figure online)



to the build-up of small amounts of 3H^+ and 4H^+ at higher acid concentrations. However, the diruthenium complexes are more fragile towards $\text{HBF}_4\cdot\text{Et}_2\text{O}$ than their iron analogues, which is evident from the reduction of peak height of their first oxidative response as the concentration of acid is increased (inset of Figs. S16, S17).

Summary and conclusions

Herein we have studied the electrochemistry of a series of structurally related diiron (**1–2**) and diruthenium (**3–4**) complexes by CV and their proton-reduction behaviour in the presence of $\text{HBF}_4\cdot\text{Et}_2\text{O}$. CVs of **1–2** in the non-coordinating solvent CH_2Cl_2 are very similar, whereas in contrast in the coordinating solvent MeCN they are significantly different. Thus, the radical anion 2^- shows greater stability in MeCN than 1^- , which we attribute to their relative rates of CO loss, being faster for 1^- . In contrast, the electrochemical response of diruthenium complexes **3–4** is essentially unaffected by the nature of solvent. Thus this study further highlights the sensitive nature of the diiron core of dithiolate-bridged complexes to small structural changes which can lead to significant differences in electrochemical responses, especially in coordinating solvents such as MeCN. Electrocatalytic studies in presence of $\text{HBF}_4\cdot\text{Et}_2\text{O}$ show that all four are catalytic towards proton reduction, the main catalytic event taking place at their first reduction potential. A smaller catalytic event is also observed at more positive potentials for all four complexes, being attributed to their partial protonation at higher acid concentrations.

Acknowledgements This research has been partly sponsored by the Ministry of Science and Technology, Government of the People's Republic of Bangladesh.

Open Access This article is distributed under the terms of the Creative Commons Attribution 4.0 International License (<http://creativecommons.org/licenses/by/4.0/>), which permits unrestricted use, distribution, and reproduction in any medium, provided you give appropriate credit to the original author(s) and the source, provide a link to the Creative Commons license, and indicate if changes were made.

References

- Georgakaki IP, Thomson LM, Lyon EJ, Hall MB, Darensbourg MY (2003) *Coord Chem Rev* 238–239:255–266
- Evans DJ, Pickett CJ (2003) *Chem Soc Rev* 32:268–287
- Rauchfuss TB (2004) *Inorg Chem* 43:14–26
- Sun L, Åkermark B, Ott S (2005) *Coord Chem Rev* 249:1653–1663
- Liu X, Ibrahim SK, Tard C, Pickett CJ (2005) *Coord Chem Rev* 249:1641–1652
- Capon J-F, Gloaguen F, Schollhammer P, Talarmin J (2005) *Coord Chem Rev* 249:1664–1676
- Siegbahn PEM, Tye JW, Hall MB (2007) *Chem Rev* 107:4414–4435
- Lubitz W, Reijerse E, van Gestel M (2007) *Chem Rev* 107:4331–4365
- Wang N, Wang M, Chena L, Sun L (2013) *Dalton Trans* 42:12059–12071
- Schmidt M, Contakes SM, Rauchfuss TB (1999) *J Am Chem Soc* 121:9736–9737
- Borg SJ, Behrning T, Best SP, Razavet M, Liu X, Pickett CJ (2004) *J Am Chem Soc* 126:16988–16999
- Felton GAN, Petro BJ, Glass RS, Lichtenberger DL, Evans DH (2009) *J Am Chem Soc* 131:11290–11291
- de Carcer IA, DiPasquale A, Rheingold AL, Heinekey DM (2006) *Inorg Chem* 45:8000–8002
- Borg SJ, Tye JW, Hall MB, Best SP (2007) *Inorg Chem* 46:384–394
- Li H, Rauchfuss TB (2002) *J Am Chem Soc* 124:726–727
- Felton GAN, Vannucci AK, Chen J, Lockett LT, Okumura N, Petro BJ, Zakai UI, Evans DH, Glass RS, Lichtenberger DL (2007) *J Am Chem Soc* 129:12521–12530

17. Capon J-F, Gloaguen F, Schollhammer P, Talarmin J (2004) *J Electroanal Chem* 566:241–247
18. Capon J-F, Gloaguen F, Schollhammer P, Talarmin J (2006) *J Electroanal Chem* 595:47–52
19. Singh PS, Christian Rudbeck H, Huang P, Ezzaher S, Eriksson L, Stein M, Ott S, Lomoth R (2009) *Inorg Chem* 48:10883–10885
20. Liu YC, Chu K-T, Huang Y-L, Hsu C-H, Lee G-H, Tseng M-C, Chiang M-H (2016) *ACS Catal* 6:2559–2576
21. Matthews SL, Heinekey DM (2010) *Inorg Chem* 49:9746–9748
22. Matthews SL, Heinekey DM (2011) *Inorg Chem* 50:7925–7927
23. Charreteur K, Kdider M, Capon J-F, Gloaguen F, Pétilion FY, Schollhammer P, Talarmin J (2010) *Inorg Chem* 49:2496–2501
24. Adam FA, Hogarth G, Richards I (2007) *J Organomet Chem* 692:3957–3968
25. Adam FA, Hogarth G, Kabir SE, Richards I (2008) *C R Chim* 11:890–905
26. Hogarth G, Kabir SE, Richards I (2010) *Organometallics* 29:6559–6568
27. Gao W, Ekström J, Liu J, Chen C, Eriksson L, Weng L, Åkermark B, Sun L (2007) *Inorg Chem* 46:1981–1991
28. Ghosh S, Hogarth G, Hollingsworth N, Holt KB, Richards I, Richmond MG, Sanchez BE, Unwin D (2013) *Dalton Trans* 42:6775–6792
29. Ghosh S, Hogarth G, Hollingsworth N, Holt KB, Kabir SE, Sanchez BE (2014) *Chem Commun* 50:945–947
30. Ridley F, Ghosh S, Hogarth G, Hollingsworth N, Holt KB, Unwin D (2013) *J Electroanal Chem* 703:14–22
31. Ghosh S, Sanchez BE, Richards I, Haque MN, Holt KB, Richmond MG, Hogarth G (2016) *J Organomet Chem* 812:247–258
32. Ghosh S, Rahaman A, Holt KB, Nordlander E, Richmond MG, Kabir SE, Hogarth G (2016) *Polyhedron* 116:127–135
33. Rana S, Ghosh S, Hossain MK, Rahaman A, Hogarth G, Kabir SE (2016) *Trans Met Chem* 41:933–942
34. Song L-C, Li C-G, Ge J-H, Yang Z-Y, Wang H-T, Zhang J, Hu Q-M (2008) *J Inorg Biochem* 102:1973–1979
35. Adam FI, Hogarth G, Richards I, Sanchez BE (2007) *Dalton Trans* 24:2495–2498
36. Hogarth G, Richards I (2007) *Inorg Chem Commun* 10:66–70
37. Lyon EJ, Georgakaki IP, Reibenspies JH, Darensbourg MY (1999) *Angew Chem Int Ed* 38:3178–3180
38. Lyon EJ, Georgakaki IP, Reibenspies JH, Darensbourg MY (2001) *J Am Chem Soc* 123:3268–3278
39. Zhao X, Georgakaki IP, Miller ML, Yarbrough JC, Darensbourg MY (2001) *J Am Chem Soc* 123:9710–9711
40. Zhao X, Georgakaki IP, Miller ML, Mejia-Rodriguez R, Chiang C-Y, Darensbourg MY (2002) *Inorg Chem* 41:3917–3928
41. Chong D, Georgakaki IP, Mejia-Rodriguez R, Sanabria-Chinchilla J, Soriaga MP, Darensbourg MY (2003) *Dalton Trans* 21:4158–4163
42. Mejia-Rodriguez R, Chong D, Reibenspies JH, Soriaga MP, Darensbourg MY (2004) *J Am Chem Soc* 126:12004–12014
43. Gloaguen F, Lawrence JD, Rauchfuss TB (2001) *J Am Chem Soc* 123:9476–9477
44. Gloaguen F, Lawrence JD, Rauchfuss TB, Bénard M, Rohmer M-M (2002) *Inorg Chem* 41:6573–6582
45. Nehring J, Heinekey DM (2003) *Inorg Chem* 42:4288–4292
46. Gloaguen F, Morvan D, Capon J-F, Schollhammer P, Talarmin J (2007) *J Electroanal Chem* 603:15–20
47. Capon J-F, Hassnaoui SE, Gloaguen F, Schollhammer P, Talarmin J (2005) *Organometallics* 24:2020–2022
48. Morvan D, Capon J-F, Gloaguen F, Le Goff A, Marchivie M, Michaud F, Schollhammer P, Talarmin J, Yaouanc J-J, Pichon R, Kervarec N (2007) *Organometallics* 26:2042–2052
49. Ezzaher S, Capon J-F, Gloaguen F, Petillon FY, Schollhammer P, Talarmin J, Pichon R, Kervarec N (2007) *Inorg Chem* 46:3426–3428
50. Gao W, Liu J, Åkermark B, Sun L (2006) *Inorg Chem* 45:9169–9171
51. Gao W, Liu J, Åkermark B, Sun L (2007) *J Organomet Chem* 692:1579–1583
52. Dong W, Wang M, Liu T, Liu X, Jin K, Sun L (2007) *J Inorg Biochem* 101:506–513
53. Chen M-H, Lin J-H, Li C-R, Gliniak J, Chang C-H, Peng C-S, Chen Y-T, Yu J-S, Wu T-K (2017) *Int J Hyd Energy* 42:9784–9794
54. Justice AK, Linck RC, Rauchfuss TB (2006) *Inorg Chem* 45:2406–2412
55. Justice AK, Linck RC, Rauchfuss TB, Wilson SR (2004) *J Am Chem Soc* 126:13214–13215
56. Chang C-H, Chen M-H, Du W-S, Gliniak J, Lin J-H, Wu H-H, Chan H-F, Yu J-S, Wu T-K (2015) *Chem Eur J* 21:6617–6622
57. Hossain GMG, Hyder MI, Kabir SE, Malik KMA, Miah MA, Siddiquee TA (2003) *Polyhedron* 22:633–640